Journal of Sound and Vibration 332 (2013) 184–198

Contents lists available at SciVerse ScienceDirect

Journal of Sound and Vibration

journal homepage: www.elsevier.com/locate/jsvi

Multi-resonant scatterers in sonic crystals: Locally multi-resonant acoustic metamaterial

V. Romero-García [a,*], A. Krynkin [b], L.M. Garcia-Raffi [c], O. Umnova [b], J.V. Sánchez-Pérez [d]

[a] Instituto de investigación para la gestión integrada de zonas costeras, Universitat Politècnica de València, Paranimf 1, 46730 Gandia, Spain
[b] Acoustics Research Centre, The University of Salford, Salford, Greater Manchester, UK
[c] Instituto Universitario de Matemática Pura y Aplicada, Universitat Politècnica de València, Camino de Vera s/n, 46022 Valencia, Spain
[d] Centro de Tecnologías Físicas: Acústica, Materiales y Astrofísica, Universitat Politècnica de València, Camino de Vera s/n, 46022 Valencia, Spain

ARTICLE INFO

Article history:
Received 13 April 2011
Received in revised form
1 August 2012
Accepted 8 August 2012
Handling Editor: Y. Auregan
Available online 12 September 2012

ABSTRACT

An acoustic metamaterial made of a two-dimensional (2D) periodic array of multi-resonant acoustic scatterers is analyzed both experimentally and theoretically. The building blocks consist of a combination of elastic beams of low-density polyethylene foam (LDPF) with cavities of known area. Elastic resonances of the beams and acoustic resonances of the cavities can be excited by sound producing several attenuation peaks in the low frequency range. Due to this behavior the periodic array with long wavelength multi-resonant structural units can be classified as a locally multi-resonant acoustic metamaterial (LMRAM) with strong dispersion of its effective properties.The results presented in this paper could be used to design effective tunable acoustic filters for the low frequency range.

1. Introduction

Recent success in the design of artificial electromagnetic materials with properties not found in nature, denoted metamaterials [1–3], has boosted a great amount of effort to develop their acoustic analogues, i.e. acoustic metamaterials [4,5]. It has been shown that periodic distributions of sound scatterers in a fluid, known as sonic crystals (SCs), can be employed in the design of acoustic metamaterials [6–8] in the low frequency regime. When sound wavelength, λ, is long compared to the separation between the scatterers, a, (long wavelength regime), homogenization theories can be applied and as a consequence SCs behave as effective homogeneous acoustic media [6] called metamaterial. However, in the diffraction regime, i.e. when $\lambda \simeq a$, both theoretical predictions and experimental results have shown, among other properties, that SCs present ranges of frequencies related to the periodicity of the structure, known as band gaps (BG), in which sound propagation is not allowed [9–12].

The pioneering work of Liu et al. [4] described a three-dimensional (3D) periodic array of coated spheres that exhibited attenuation bands with wavelength about two orders of magnitude larger than the periodicity of the structure. The origin of this phenomenon has been explained by means of the localized resonances associated with each scatterer: the hybridization of the flat resonance band and the propagating band of the periodic medium produces the stop band. Thus, the frequency of the stop band can be tuned by varying the size and geometry of the resonator. The sound attenuation

* Corresponding author.
E-mail addresses: virogar1@mat.upv.es, virogar1@gmail.com (V. Romero-García), A.Krynkin@salford.ac.uk (A. Krynkin), lmgarcia@mat.upv.es (L.M. Garcia-Raffi), O.Umnova@salford.ac.uk (O. Umnova), jusanc@fis.upv.es (J.V. Sánchez-Pérez).
URL: http://personales.upv.es/virogar1 (V. Romero-García).

0022-460X/$ - see front matter © 2012 Elsevier Ltd. All rights reserved.
http://dx.doi.org/10.1016/j.jsv.2012.08.003

level in this stop band also increases with the number of local resonators. In such a way, Liu et al. showed a general direction towards the design of locally resonant acoustic metamaterials (LRAM) where the effective properties can be used to accurately describe the wave interaction with LRAM.

The sound speed in the LRAM is equal to $\sqrt{\kappa_{\text{eff}}/\rho_{\text{eff}}}$, where κ_{eff} and ρ_{eff} are the effective bulk modulus and the mass density, respectively. In conventional acoustic materials, the real part of κ and ρ is always positive which allows maintaining structural stability. This is not necessarily the case for LRAM. It has been previously shown that in periodic media made of resonant scatterers, the effective density becomes negative near resonant frequencies, giving rise to exponential decay of the waves [13]. This is in contrast to the case of SC formed by rigid scatterers where the effective properties are real and positive and can be used, for example, to design gradient index lenses [7].

In last years, several 3D [14] and 2D [15] locally resonant phononic crystals have been analyzed, showing the resonance gaps and the almost dispersionless bands within the absolute gap originated from the resonance modes of the individual scatterers. Numerical simulations showed the tunability of the frequency position of these resonances by a proper choice of the different parameters involved; size of cavities, nature of gases inside and outside the scatterer, and elastic coefficients of the solid material. Very recent works have demonstrated the existence of both electromagnetic [16] and elastic [17] metamaterials with multiple resonances. Lai et al. [17] designed an elastic metamaterial exhibiting multiple resonances in its building blocks. These metamaterials could be used as wave polarizers or for imaging and controlling seismic waves. For the electromagnetic counterpart, Turkmen et al. [16] experimentally and theoretically analyzed a compact multi-resonant metamaterial structure based on U- and T-shaped nano-apperture antennas, showing opportunities in applications ranging from subwavelength optics and optoelectronics to chemical and biosensing.

In the present work an acoustic metamaterial made of a two-dimensional (2D) periodic array of scatterers exhibiting multi-resonant acoustic behavior in the long wavelength regime is studied. A scatterer with multiple resonances of different nature is used to design a locally multi-resonant acoustic metamaterial (LMRAM). The building blocks of this LMRAM consist of a combination of elastic beams of low-density polyethylene foam (LDPF) with cavities of known area. The conventional application of LDPF can be found in packaging industry or in shock absorbing and vibration damping techniques. The low density, the elastic properties of this material as well as the shape of the scatterer allow the sound to excite both elastic resonances of the material and acoustic cavity resonances producing several attenuation peaks in the low frequency range.

The work is organized as follows. First, in Section 2 some of the experimental results that motivate this work are presented. The acousto-elastic coupled problems for the complex geometry of the real scatterer are solved in Section 3. The behavior of both single scatterers and the periodic arrangements of scatterers are analyzed using finite element method (FEM). The details of the experimental setup and the experimental validation of all the numerical simulations are described in Section 4. The performance of the periodic structure in the long wavelength regime is discussed in Section 5. Sound manipulation is perhaps the most obvious application of the structures presented in this work, and a discussion of this application is presented in Section 6. Finally, a summary of results as well as the conclusions of the work are presented.

2. Motivation

The scatterers analyzed in this work will be called U-profiles due to their geometrical shape (see Fig. 1a). The goal of this section is to describe the system to be analyzed, showing some of the experimental results that motivated the work. Further details of the experimental setup will be given later (Section 4).

Fig. 1a shows the measured acoustic response of a commercial scatterer made of LDPF (see inset). The insertion loss (IL) defined as the difference between the sound pressure level (SPL) recorded without and with the sample has been measured. The red dashed line in Fig. 1a illustrates the IL of a single U-profile. One can observe two attenuation peaks around 700 Hz and 1100 Hz. These peaks, when the U-profiles are arranged in a lattice – periodic medium – forming a SC, will give rise to a couple of attenuation bands that we will call first and second attenuation bands, respectively. Their nature can be understood as elastic and cavity resonances of every scatterer in the SC as will be shown later.

With these scatterers, an array with triangular unit cell which lattice constant is $a=0.127$ m, as shown in Fig. 1b, has been built. Pictures of both the cross-section and the complete SC are shown in Fig. 1b. For this array the Bragg frequency ($f_{\text{Bragg}} = c_{\text{host}}/2a$, $c_{\text{host}} = 340$ m/s) is 1545 Hz. The goal of this work is the analysis of the effect of the resonances of the building blocks on the propagation properties of the periodic structure. Hereinafter, we will pay attention to the range of frequencies below the first Bragg peak of the periodic structure. Fig. 1c and d shows the IL measured 1 m behind a SC made of U-profiles for two different incidence directions 0° and 30°, respectively. One can see three attenuation bands, two corresponding to the resonances of the scatterers (700 Hz and 1100 Hz) and the one corresponding to the periodicity (1545 Hz) in the diffraction regime.

3. Numerical results

In this section the resonances of a single U-profiles and the band structures of their periodic arrays are analyzed numerically using FEM. We use COMSOL Multiphysics software working together with MATLAB. The FEM is an adequate technique when the shape of the modeled objects is complicated and when several physical problems are coupled.

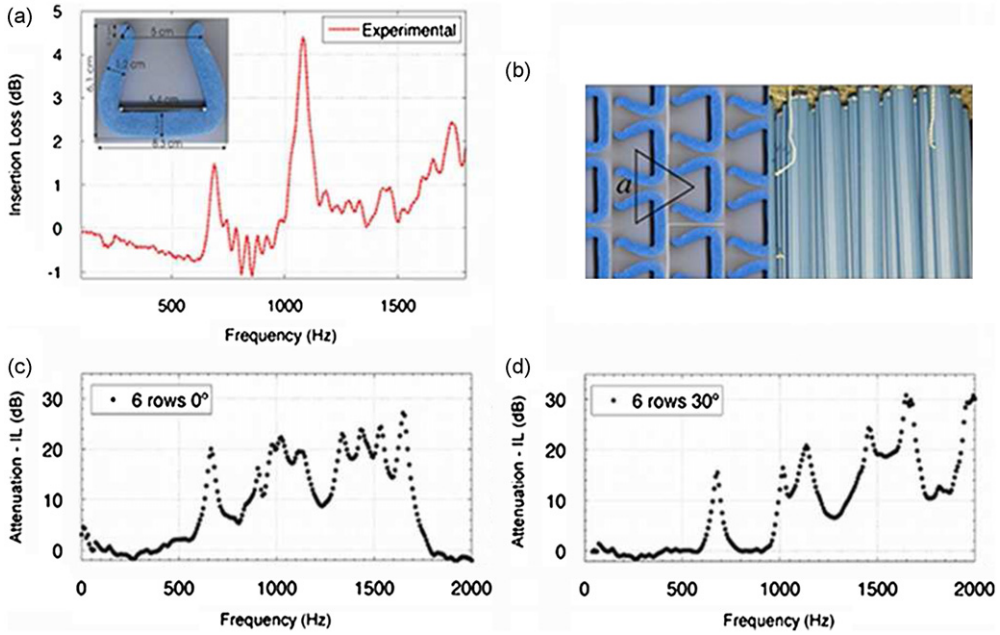

Fig. 1. Experimental results. (a) IL of single U-profile. (b) Pictures of both the cross-section and the complete structure used in the experimental setup. Details of the triangular unit cell are also shown. (c) and (d) measured IL of a SC made of U-profiles arranged in a triangular array, lattice constant $a=0.127$ m, measured at 0° and 30°, respectively. The inset shows the transversal view of a U-profile. (For interpretation of the references to color in this figure caption, the reader is referred to the web version of this article.)

Although this numerical approximation takes into account the complex geometry of the scatterers, a simplified physical analysis can be done and, as a consequence, approximate equations of the resonances are obtained. More details of this phenomenological analysis can be found in Appendix A.

3.1. FEM model: acousto-elastic coupling

This section starts with the analysis of acoustic wave propagation inside a periodic structure made of solid scatterers, B, embedded in a fluid host, A, using FEM. If the host material is fluid only longitudinal waves are supported by the structure. Then, the governing equation in A is

$$-\frac{\omega^2}{c_A^2}p=\nabla\left(\frac{1}{\rho_A}\nabla p\right), \tag{1}$$

where p is the pressure, $\omega=2\pi f$ with f the frequency, ρ_A is the density and c_A is the sound velocity in the host material.

The propagation of elastic waves inside the scatterers is governed by

$$-\rho_B\omega^2 u_i=\left\{\frac{\partial\sigma_{ij}}{\partial x_j}\right\}, \tag{2}$$

where ρ_B is the density of the elastic material and u_i is the ith component of the displacement vector, $\mathbf{u}$. The stress tensor is defined by

$$\begin{aligned}\sigma_{ij}&=\lambda_B u_{ll}\delta_{ij}+2\mu_B u_{ij},\\ u_{ij}&=\frac{1}{2}\left\{\frac{\partial u_i}{\partial x_j}+\frac{\partial u_j}{\partial x_i}\right\},\end{aligned} \tag{3}$$

where λ_B and μ_B are the Lamé coefficients which are related to the longitudinal, c_l, and transversal, c_t, sound velocities in the solid as

$$c_l=\sqrt{\frac{\lambda_B+2\mu_B}{\rho_B}}, \tag{4}$$

$$c_t=\sqrt{\frac{\mu_B}{\rho_B}}. \tag{5}$$

On the other hand, the Lamé coefficients can be also related to Young's modulus, E, and Poisson's ratio, v, as follows:

$$\lambda_B = \frac{Ev}{(1+v)(1-2v)}, \tag{6}$$

$$\mu_B = \frac{E}{2(1+v)}. \tag{7}$$

In this coupled problem the acoustic wave is incident on the scatterer and then the pressure acts as a load on the elastic medium. In order to simultaneously solve (1) and (2) the following boundary conditions have been applied:

$$\frac{\partial p}{\partial n}\Big|_{\partial B} = \rho_A \omega^2 \mathbf{un},$$
$$\sigma_{ij} n_j\Big|_{\partial B} = -p n_i. \tag{8}$$

where ∂B is the boundary of medium B and $\mathbf{n}$ is the unit vector normal to the scatterer surface and directed outward. In the numerical problem, the solution domain was surrounded by perfectly matched layer (PML) [18] region in order to emulate the Sommerfeld radiation condition.

3.2. Scattering problem

3.2.1. Single scatterer

First of all, the frequency response of the U-profile will be analyzed. The real geometry of the U-profiles was approximated using the CAD tools of COMSOL. The scatterer is shown in the inset in Fig. 2. In this section a plane wave impinging the scatterer from the left is considered and the IL is evaluated behind the scatterer. The physical properties of the LDPF are shown in Table 1.

The blue continuous line in Fig. 2 shows the numerical results. The frequency response obtained numerically is close to the experimental results which is plotted using a red dashed line in Fig. 2. Two attenuation bands can be observed near 700 Hz, corresponding to the elastic resonances (continuous arrow), and near 1300 Hz, corresponding to cavity resonances (dashed arrow).

Fig. 2 shows a difference between the numerical results and data for the frequencies of the second peak (cavity resonance shown by dashed arrow in Fig. 2). FEM model should be capable of describing any effects within the theory of linear acoustic and solid mechanics, therefore any discrepancies between numerical results and the data are most likely to

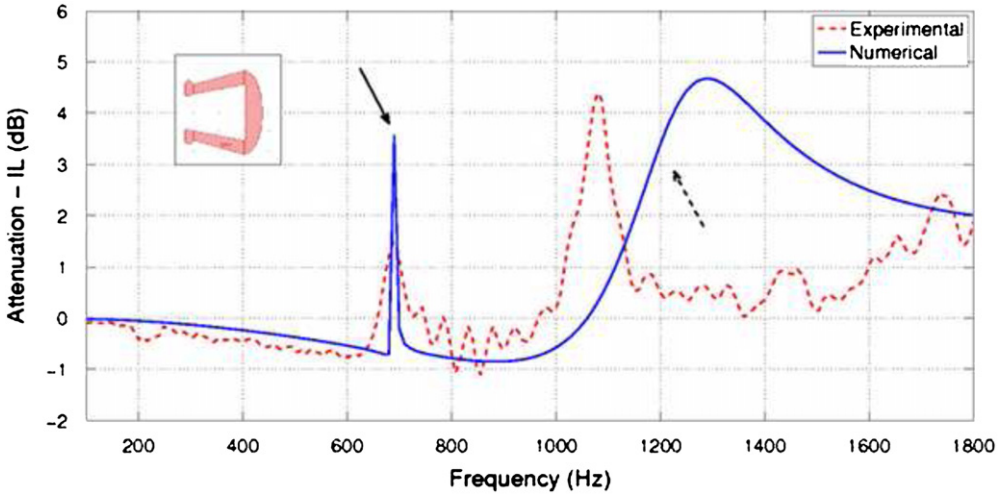

Fig. 2. IL produced by a single U-profile. Numerical predictions (red dashed line) and experimental results (blue continuous line). Continuous (Dashed) arrow shows the elastic (cavity) resonance peak. The insets show the geometry used in the numerical model. (For interpretation of the references to color in this figure caption, the reader is referred to the web version of this article.)

Table 1
Physical parameters of the LDPF.

Density, ρ_B (kg/m^3)	Young's modulus, E (10^9 Pa)	Poisson's ratio, v
50	0.095	0.32

be due to the idealization of the scatterer material and possible differences in the geometry. It should be noted that the resonances of the U-profile depend on both the aperture of the cavity and the length of its elastic lateral walls. The observed elastic resonance is very sensitive to the length of the beams while the observed cavity resonance is very sensitive to the area of the cavity (see Eqs. (A.3), (A.4) and (A.8) in Appendix A). This gives the possibility to tune the frequency response of the two resonances in the long wavelength regime of the periodic medium formed using these elements.

3.3. Infinite periodic array of U-profiles

A band structure of the periodic arrangement of U-profiles is analyzed applying Bloch periodic boundary conditions for a unit cell. The left panel of Fig. 3 shows the band structures of a periodic arrangement of U-profiles arranged in a triangular lattice with lattice constant $a=0.127$ m. For further analysis the band structure of a SC made of rigid U-profiles (black dashed lines) is also plotted in order to be compared with that of a periodic array of elastic U-profiles (blue continuous lines). For the perfectly rigid U-profiles Neumann boundary conditions have been applied on the walls of the scatterer. One can observe that the arrangement of rigid U-profiles presents the BG related to the periodicity ($\simeq 1545$ Hz) as well as the stop band due to the cavity resonance (1155 Hz). However, for the SC made of elastic U-profiles (blue continuous lines) one can observe the BG due to the periodicity ($\simeq 1545$ Hz) and the stop bands due to both the resonance of the cavity (1155 Hz) and the resonance of the EB (700 Hz). The non-propagating ranges of frequencies are marked by the black rectangles.

In order to compare the numerical results with the data, a plot has been added in the right panel of Fig. 3 showing the measured IL of a triangular periodic distribution of elastic U-profiles along the main symmetry directions: 0° (blue line) and 30° (red dashed line). The SC used in the experimental setup is formed by 6 rows of 10 scatterers per row. One can observe the weak dependence of the resonances on the direction of incidence. However, as it is predicted for periodic structures [12], the range of attenuated frequencies depends on the incident direction (it is said that different pseudogaps appear at ΓX and ΓJ directions, being the intersection of both pseudogaps the BG of the structure). It is worth noting that the measured IL presents a background attenuation possibly due to the losses in the material (discussed later in Section 4). Recent works [19,20] analyze the effect of the losses of the scatterers on the band structure of the periodic systems. Generally speaking, these losses depend on the frequency and one should analyze the complex band structures [19] solving for the inverse problem $k(\omega)$. We have not considered them in the analysis of the periodic structure because the methodology is out of the scope of the present work; however, the losses of the material are discussed in the next Section 4 showing the influence of these effects on the results shown in the work.

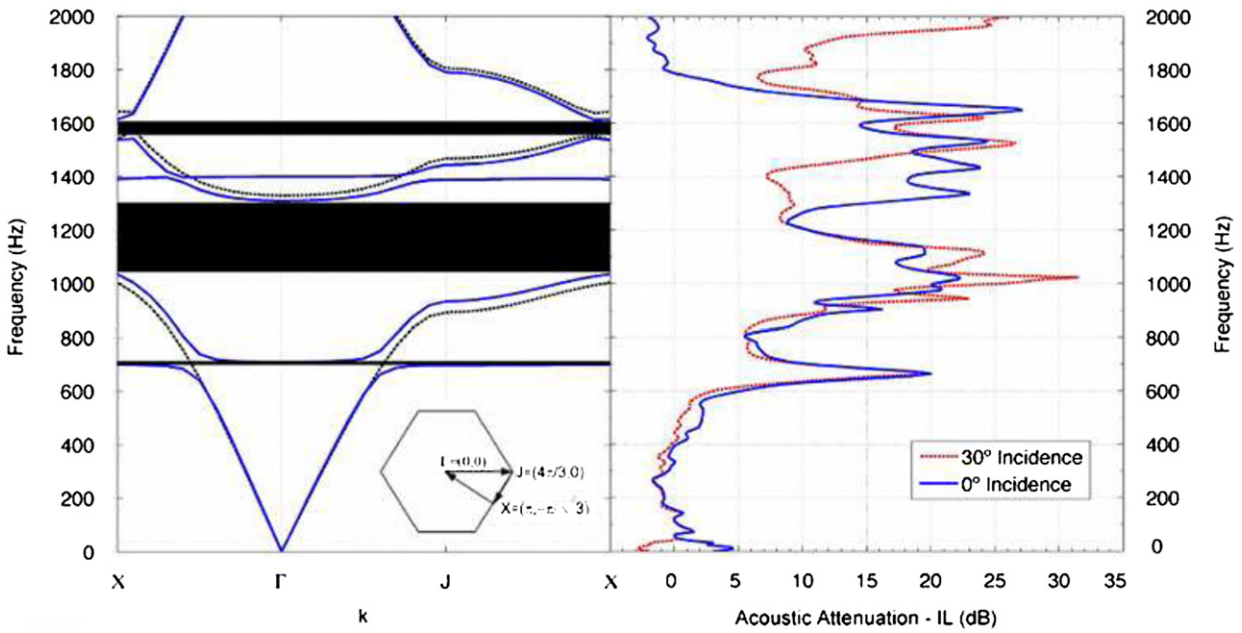

Fig. 3. Band structure for a periodic arrangement of U-profiles in triangular lattice with $a=0.127$ m. Left panel: rigid U-profiles (black dashed line) and elastic U-profiles (blue continuous line). The non-propagating ranges of frequencies are shaded in black.. The Brillouin zone is defined as $\Gamma=(0,0)$, $X=(\pi,-\pi/\sqrt{3})$, $J=(4\pi/3,0)$. Right panel: measured IL of a triangular array made of 6 rows of 10 U-profiles measured in the two main symmetry directions, 0° (blue line) and 30° (red dashed line). We can observe that both the number of attenuation peaks and their position are in very good agreement with the elastic U-profiles. (For interpretation of the references to color in this figure caption, the reader is referred to the web version of this article.)

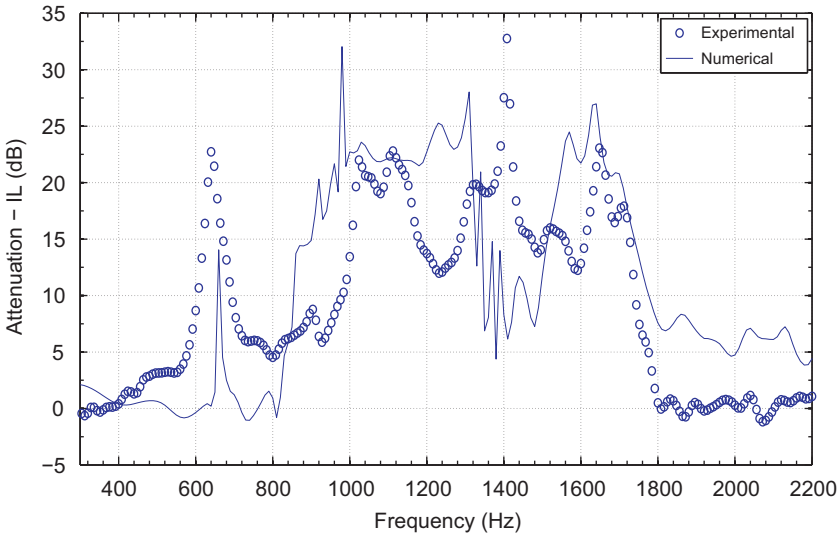

Fig. 4. IL of an array of U-profiles. Numerical predictions are shown with blue continuous line and open circles represent the measured IL. A plane wave impinges the structure from the left side. (For interpretation of the references to color in this figure caption, the reader is referred to the web version of this article.)

3.3.1. *Finite periodic array of U-profiles*

The next step is to analyze a finite periodic array of elastic U-profiles arranged in a triangular lattice with lattice constant $a=0.127$ m. Here, a plane wave impinging from the left side is considered and the numerical domain is surrounded by PML. Thus the numerical solution satisfies an approximated Sommerfeld condition.

The numerically predicted IL of a finite structure made of 6 rows of 10 U-profiles for an incident wave in the direction of 0° is shown by a blue continuous line in Fig. 4. By comparing these results with those for a single U-profile (see Fig. 2), one can conclude that the attenuation level at the resonant frequencies of both the EB and the cavity grows as the number of scatterers increases. Moreover, an attenuation band around the Bragg frequency (1545 Hz) appears, which is related to the array periodicity.

The measured IL for this array is shown by open circles in Fig. 4. A good correspondence between numerical predictions and the data can be observed. Several discrepancies between them appear around 1400 Hz. As mentioned in the previous sections they could be due to the idealization of the scatterer material and the possible differences in the geometry.

Some works [21,22] show that resonances can be used to increase the attenuation within BG frequency range using resonators with the resonance near Bragg's frequency. In this work the possibility to combine Bragg's effect with the low frequency multiple resonances is demonstrated, so that these phenomena are well separated in frequencies.

4. Experimental results

The experimental setup as well as the experimental validation of the theoretical predictions are described in this part of the work.

4.1. *Experimental setup*

The experimental results have been obtained under controlled conditions in an echo-free chamber. Data acquisition is performed by a prepolarized free-field microphone 1/2 in Type 4189 B&K. The microphone position is varied by using a Cartesian robot which controls the movement along the three axes (*OX*, *OY* and *OZ*), installed in the ceiling of the echo-free chamber. 3D Robotized e-Acoustic Measurement System (3DReAMS) has been designed to sweep the microphone through a 3D grid of measuring points located on any trajectory inside the chamber. The source GENELEC 8040A is used to produce white noise. This source is an active monitoring loudspeaker designed to produce high sound pressure level output, low coloration and broad bandwidth in a small enclosure size. When the robotized system is turned off, the microphone acquires the temporal signal. This signal is saved on a computer and then, using the fast Fourier transform (FFT), the power spectra, the frequency response or the sound level measurements can be obtained. National Instruments cards PCI-4474 and PCI-7334 have been used together with the Sound and Vibration Toolkit and the Order Analysis Toolkit for LabVIEW for both the data acquisition and the motion of the robot. Fig. 5 shows the experimental setup as it is placed in our echo-free chamber.

The analysis of wall vibrations has been performed using a miniature accelerometer B&K Type 4393. This accelerometer is made of Titanium whose weigh is 2.2 g (1.7 percent of the weight of the U-profiles). Type 4393 of B&K is suitable for

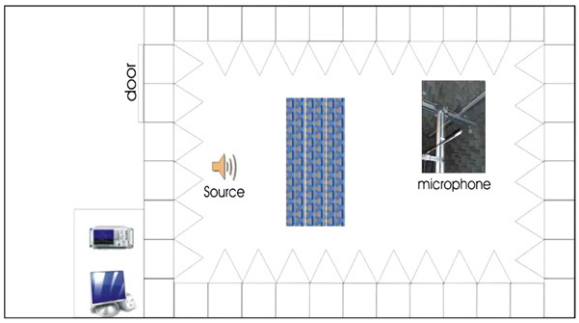

Fig. 5. Schematic view of the experimental setup.

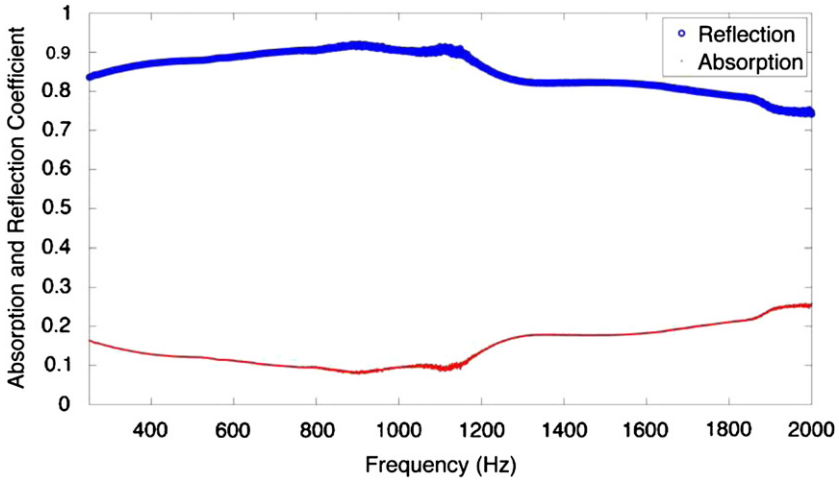

Fig. 6. Measured absorption and reflection coefficient of the low density polyethylene foam. The thickness of the sample is 1.3 cm.

measurements on lightweight structures and it was used to analyze the wall vibration of the U-profile scatterers. The typical frequency response of the Type 4393 is a flat response from 200 Hz to 18 kHz.

4.2. Material properties: absorption and reflection coefficients of LDPF

Following the standard approaches in measuring acoustic properties [23], the reflection and the absorption coefficients of the LDPF have been experimentally derived by means of the transfer function method using an impedance tube. In this methodology, the complex reflection coefficient is given by

$$R_c = \frac{H_{12} - e^{iks}}{e^{-iks} - H_{12}} e^{i2kd}, \tag{9}$$

where H_{12} is the acoustic transfer function of pressure measured at the locations of two microphones, d is the distance between the first microphone location and the test sample, and s is the microphone spacing. Using Eq. (9) the absorption coefficient α is defined by

$$\alpha = 1 - |R_c|^2. \tag{10}$$

The experimental reflection and absorption coefficients of the LDPE foam are represented in Fig. 6. The results obtained for the rectangular sample of thickness 1.3 cm are similar to those obtained in the previous works [24]. It is worth noting that according to our experimental results the acoustical properties of LDPF analyzed, these are not sensitive to a small variation of the sample thickness.

Fig. 6 shows that LDPF presents values of the absorption coefficient around 0.2 for all the complete range of frequencies analyzed in this work. Thus, the differences in the base line of attenuation between the numerical predicted IL and experimental one observed in Fig. 4 could be explained by this absorption of the material.

4.3. Single scatterer

The experimental analysis of the single LDPF scatterers has been divided into two parts, i.e. acoustic and vibrational analyzes.

In order to observe the resonances, both the vibration of the EB and the level pressure of the acoustic field inside the cavity of the U-profile have been measured using the accelerometer and microphone, respectively. In Fig. 7a the vibration of the EB for two different incidence directions of the acoustic wave is illustrated. Blue continuous line represents the vibrations of the wall of the U-profile for the incident wave in the ΓX direction. Red dashed line represents the vibrations of the walls for a wave impinging in the ΓJ direction. The vibration of the elastic walls of the U-profiles increases at the resonant frequencies. Fig. 7a shows the increase in the wall vibrations in the resonance region of the EB and near the cavity resonance independently of the incident direction of the acoustic wave.

Fig. 7b shows the pressure level inside the cavity of the LDPF obtained by moving the microphone with 3DReAMS in 0.01 m steps inside the cavity. The field measured inside the cavity is similar to the one numerically obtained. The resonance of the cavity induces the wall vibration observed in Fig. 7a (see black arrow).

At this stage we would like to point out that the height of the U-profiles is 2 m, which is much longer than the wavelength of the resonances analyzed in this work. However, we have experimentally analyzed the frequency response of several U-profiles of lesser height, observing always the same response in frequency. This result shows that the consideration of our structures as 2D is a good approximation.

4.4. Periodic array

4.4.1. Dependence on the number of resonators

One can expect that both the resonant and periodic effects depend on the number of scatterers in the array. To prove it, experiments have been carried out with six configurations, everyone with a different number of rows. The largest structure presents 6 rows of 10 scatterers per row. The IL has been measured at the same position for all six arrays with the number of rows ranging from one to six. Fig. 8 shows these experimental results. The colored lines represent the IL measured in a point located 1 m away from the edge of the complete SC. The IL of a structure made of 1 row of U-profiles for 0° (respectively, 30°) of incidence are shown by blue dots in Fig. 8a and b. The IL of a structure made of six rows of U-profiles for 0° (respectively, 30°) of incidence are shown by the black squared lines.

It can be observed that the peak heights of IL corresponding to both resonances, the elastic and the cavity ones, depend on the number of cylinders in the structure. Also, in the case of only one row, where there is no periodicity in 2D, the resonance peaks are present in the attenuation spectrum whereas Bragg's peaks do not appear. It is interesting to note that these structures do not present ranges of frequencies with sound reinforcement in the range of frequencies of interest.

4.4.2. Dependence on the incidence direction

One of the main characteristics of the BG produced by the periodicity of the arrays is their dependence on the incident direction of the wave. However, it is known that the resonant effects do not depend on the incidence direction.

Here, the dependence on the frequency response of a periodic array made of U-profiles on the direction of incidence is investigated. The IL of a complete structure for several incident directions in between the two main symmetry directions (0° and 30°) has been measured. Fig. 9 shows these experimental results.

A weak dependence of the IL peaks produced by the EB and cavity resonances can be observed in Fig. 9. However, one can see that the behavior of the attenuation peak due to array periodicity is strongly dependent on the incidence direction.

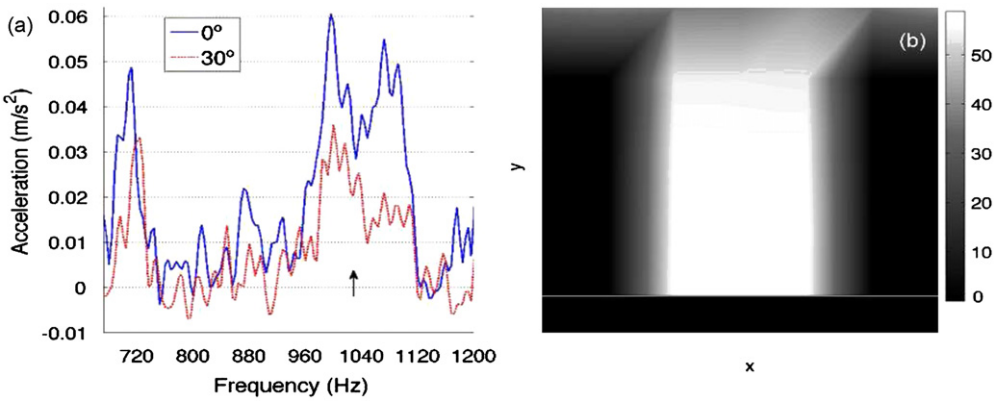

Fig. 7. Experimental results for a single scatterer. (a) Measurements of the LDPF scatterer wall vibrations. Blue line represents 0° of incidence and red dashed line represents 30° of incidence. (b) Sound level map measured inside the cavity for the resonant frequency $f=1104$ Hz. Step $\Delta x=\Delta y=0.01$ m. (For interpretation of the references to color in this figure caption, the reader is referred to the web version of this article.)

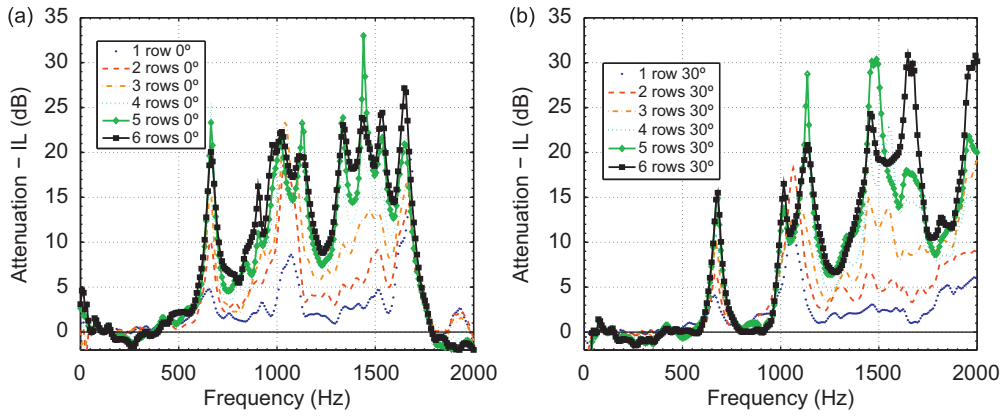

Fig. 8. Dependence of the measured IL on the number of scatterers in the array. Open colored circles represent the IL for six structures with different number of rows (from 1 to 6 rows of 10 cylinders per row). IL is measured 1 m away from the edge of the complete structure. (a) Measurements in the ΓX direction. (b) Measurements in the ΓJ direction. (For interpretation of the references to color in this figure caption, the reader is referred to the web version of this article.)

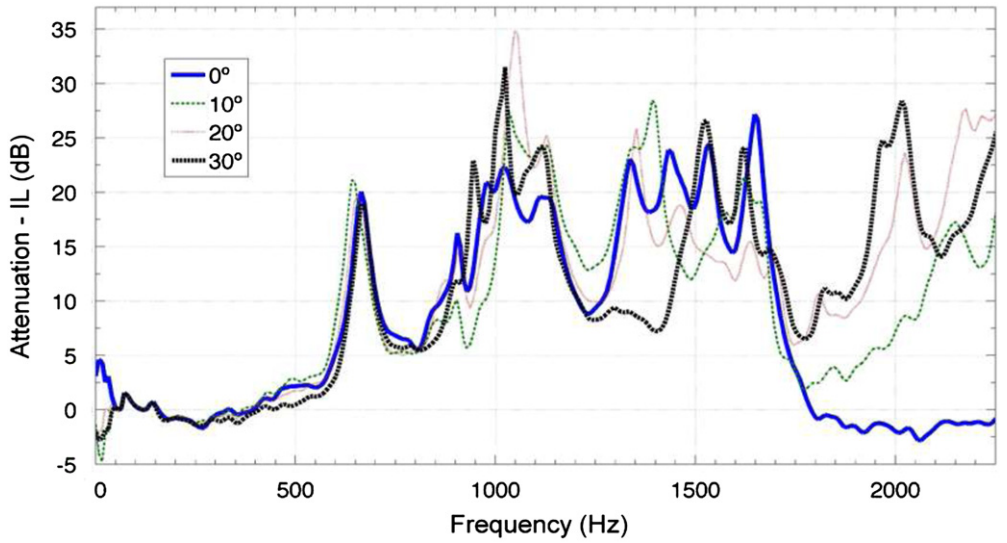

Fig. 9. Dependence of the measured IL of the complete array on the angle of incidence. Open colored circles represent the IL for four different directions, 0°, 10°, 20° and 30°. IL is measured 1 m away from the edge of the complete structure (6 rows of 10 cylinders per row). All the IL have been measured in a point placed 1 m away from the edge of the biggest structure (6 rows of 10 cylinders per row). (For interpretation of the references to color in this figure caption, the reader is referred to the web version of this article.)

5. Locally multi-resonant acoustic metamaterial

In LRAM, the sound speed is proportional to $\sqrt{\kappa_{\text{eff}}/\rho_{\text{eff}}}$, where κ_{eff} and ρ_{eff} are the effective bulk modulus and the mass density, respectively. Metamaterial frequency response depends on the values of these parameters. SC made of rigid scatterers can be considered as an acoustic metamaterial showing real and positive effective properties [7]. However, some interesting differences can appear in LRAM with negative values of the effective parameters [4]. Depending on the values of these effective parameters several effects can be observed [25].

In order to have a propagating plane wave inside the medium, either both κ_{eff} and ρ_{eff} must be positive or both of them must be negative. These two combinations give a positive effective sound speed; however, there are significant differences between the two cases. To see these differences the relative direction of the Poynting vector with respect to the wave vector should be analyzed. The Poynting vector for a propagating plane wave is defined as

$$\mathbf{S} = \frac{\mathrm{i}}{2\omega\rho} p\nabla p* = \frac{|\mathbf{p}|^2\mathbf{k}}{2\omega\rho}. \tag{11}$$

If κ_{eff} and ρ_{eff} are both positive, the Poynting vector, **S**, has the same direction as **k** and Snell's law is normally accomplished. However, if κ_{eff} and ρ_{eff} are negative, **S** and **k** have opposite directions. Physically, the negativity of both κ_{eff}

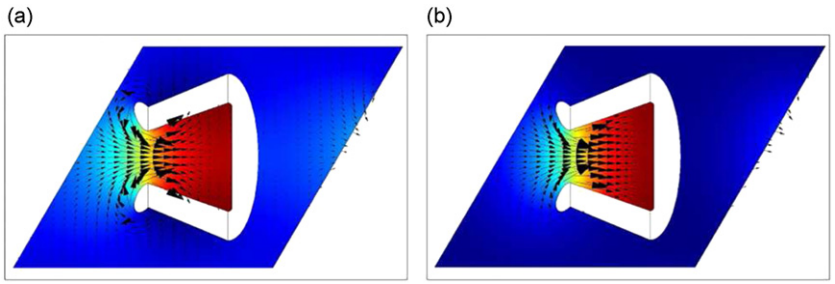

Fig. 10. Field distribution at frequencies of the (a) elastic, 700 Hz, and (b) cavity, 1155 Hz, resonances. Color scale represents the pressure field and arrows represent the particle displacement velocity field. (For interpretation of the references to color in this figure caption, the reader is referred to the web version of this article.)

and ρ_{eff} means that the medium displays an anomalous response at some frequencies such that it expands upon compression (negative bulk modulus) and moves to the left when being pushed to the right (negative density) at the same time. These double negative materials present unique properties, such as negative refractive index and subwavelength focusing [8].

However, if only one of these quantities is negative, the effective sound speed is complex valued, as is the wavenumber. Thus, when the real part of the expression for the Poynting vector is negative and sufficiently large, a frequency range where $\text{Re}(\mathbf{kS}) < 0$ is observed. A direct consequence of such behavior is the exponential wave attenuation at these frequencies. It has been previously shown that low frequency attenuation bands can be induced by an effective bulk modulus that becomes negative near the resonance frequencies, giving rise to exponential decay of modes [5].

In the system studied here, the stop bands at low frequencies are independent of both the angle of incidence and the lattice constant.[1] Moreover, as has been previously shown there is no transmission of waves at the resonant frequencies, i.e. we observe two attenuation bands for the resonant frequencies. Oppositely, we have not seen negative refraction or subwavelength imaging near the resonance. Thus, it can be concluded that, as in the case of Ref. [5], the periodic structure made of U-profile could be described as a LMRAM with one of the effective parameters being positive and the other one negative at the resonant frequencies.

At this stage we would like to remark that a rigorous parameter retrieval procedure similar to those developed for electromagnetic and acoustic cases needs to be implemented to obtain the κ_{eff} and ρ_{eff}. But since in our case the structural units of LMRAM are comparable in size with the wavelength of the operating system ($\lambda \sim a$), i.e. some of the resonances in our case are not far in the long wavelength regime, such a homogenization of all properties via effective medium parameters is difficult. However, as it has been previously done for double negative metamaterials out of the long wavelength regime in Ref. [8], we can follow the formalism previously applied to the electromagnetic metamaterial to phenomenologically analyze the behavior of the system [5] due to the fact that our system satisfy the requirements to be a single negative metamaterial as it has been previously described.

The negativity of the effective bulk modulus and the effective mass density in acoustic metamaterials is related to the monopolar and the dipolar resonances, respectively. Several acoustic metamaterials made of solid and fluid unit mixtures were proposed to obtain simultaneously negative effective mass density and bulk modulus [26]; however, the frequency band where the double negativity is achieved is usually very narrow. On the other hand cavity resonances similar to ones described in this work have been used in the previous works to design acoustic metamaterials [5,27] with negative real part of the complex valued bulk modulus at the resonance frequencies (monopolar resonance). The elastic resonances of the U-profiles correspond to vibrations of the two EB from inside to outside the cavity being the displacement practically monopolar. The monopolar behavior of the elastic and cavity resonances of building blocks of our system are shown in Fig. 10. Color scale represents the pressure field and arrows represent the particle displacement velocity field. Then, due to the fact that the negativity of the bulk modulus corresponds to monopolar resonances one can use the effective bulk modulus to describe the LMRAM. The agreement between the predictions and the experimental results shown in Fig. 11 justify the validity of this approach for the problem considered.

The acoustic properties of a 2D SC can be mapped into an electromagnetic counterpart, where p, $\mathbf{v}$, ρ, k correspond to H_z, $\mathbf{E}$, ε, μ, respectively. Following the formalism of the electromagnetic metamaterials, one can consider that the systems behave as a metamaterial with an effective bulk modulus $\kappa_{\text{eff}}(\omega)$ in the form,

$$\kappa_{\text{eff}}^{-1}(\omega) = \sum_{j=1}^{N_{\text{res}}} \left(\frac{E}{3(1-2\nu)}\right)^{-1} \left(1 - \frac{F\omega_{0j}^2}{\omega^2 - \omega_{0j}^2 + \mathrm{i}\Gamma\omega}\right), \tag{12}$$

where F is the filling fraction, ω_{0j} represents the resonant frequencies of the LDPF scatterer, Γ is the dissipation loss in the resonating elements and N_{res} is the number of resonances of the scatterers. In our system $N_{\text{res}} = 2$ and the resonant

[1] We have also experimentally observed no dependence on the height of the U-profiles.

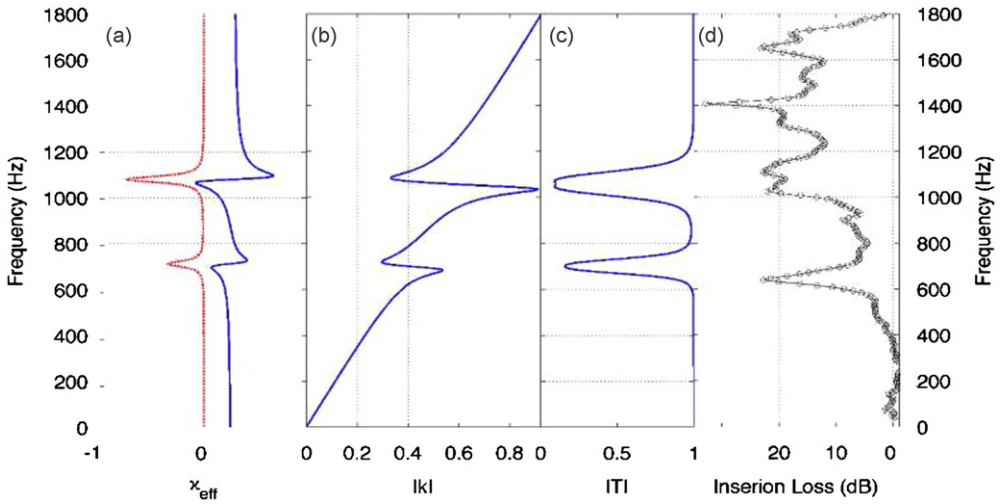

Fig. 11. Effective properties of the LMRAM. (a) Effective bulk modulus. Imaginary part is plotted in red dashed line whereas real part is plotted in blue continuous line. (b) Dispersion relation. (c) Transmission coefficient for a slab of metamaterial with $L_{\text{eff}} = 0.549$ m. (d) Measured IL of an array of U-profiles. (For interpretation of the references to color in this figure caption, the reader is referred to the web version of this article.)

frequencies can be obtained from Eqs. (A.3) and (A.4) as

$$\omega_{01} = \frac{\sqrt{12}}{l_x^2}\left(\frac{\rho l_x t_1}{EI}\right)^{-1/2}, \tag{13}$$

$$\omega_{02} = \frac{2\pi c_{\text{air}}}{4(l_x+\delta)}. \tag{14}$$

In Fig. 11a, the effective bulk modulus of the material is presented. Its imaginary part presents a frequency-dependent response which is essential to explain the appearance of stop bands in the same range of frequencies.

To obtain the transmission coefficient of a slab of metamaterial with the bulk modulus defined by Eq. (12), it is necessary to determine the effective slab thickness. The filling fraction of the structure is

$$F = \frac{\sum_{i=1}^{N} A_{\text{cyl}}}{A_{\text{eff}}}, \tag{15}$$

where N is the number of scatterers, A_{cyl} is the area of each scatterer and A_{eff} is the area occupied by the slab of the homogeneous material. For a slab composed of N scatterers of area A_{cyl} arranged in a lattice with unit cell area A_{uc}, the filling fraction is given by the following equation:

$$\frac{A_{\text{cyl}}}{A_{\text{uc}}} = \frac{NA_{\text{cyl}}}{A_{\text{eff}}}. \tag{16}$$

For the homogenized system with the rectangular shape considered in this work (6 rows of 10 scatterers with triangular periodicity), the effective thickness L_{eff} is

$$L_{\text{eff}} = 5\frac{\sqrt{3}a}{2}. \tag{17}$$

For the parameters considered in this work, $L_{\text{eff}} = 0.549$ m.

Finally, the effective dynamic mass density,

$$\frac{\rho_{\text{eff}}}{\rho_{\text{h}}} = \frac{\rho_{\text{h}}+\rho_{\text{s}}-F(\rho_{\text{h}}-\rho_{\text{s}})}{\rho_{\text{h}}+\rho_{\text{s}}+F(\rho_{\text{h}}-\rho_{\text{s}})}, \tag{18}$$

where ρ_{s} is the density of the scatterer and ρ_{h} is the density of the host material.

It would be interesting to know the dispersion for a medium with negative elastic bulk modulus. In the low frequency range, the real ($x = \text{Re}(\kappa)$) and imaginary ($y = -\text{Im}(\kappa)$) parts of the bulk modulus can be related to the propagation constant of the media as [5]

$$\text{Re}(k) = -\frac{\omega}{2}\sqrt{\frac{\rho}{x^2+y^2}}\left(\sqrt{x^2+y^2}-x\right)^{1/2}, \tag{19}$$

$$\text{Im}(k) = \frac{\omega}{2}\sqrt{\frac{\rho}{x^2+y^2}}\left(\sqrt{x^2+y^2}+x\right)^{1/2}. \tag{20}$$

Using the effective elastic bulk modulus defined in Eq. (12) the dispersion relation can be calculated making use of Eqs. (19) and (20). In Fig. 11b, one can see the dispersion relation obtained for the effective medium. Two spectral bands of non-propagating modes are expected in the vicinity of the resonances of the structural units.

The transmission coefficient of a slab of 0.549 m of the acoustic metamaterial has been calculated as described in [28]. In Fig. 11c, the absolute value of the transmission coefficient is shown. One can observe a reduction in transmission around the resonant frequencies.

In Fig. 11d, IL data for a periodic array of U-profiles arranged in a triangular lattice are presented. The attenuation peaks predicted by the effective medium approximation correspond to those observed in experiments.

6. Applications: tunable acoustic filters

Sound manipulation is perhaps the most obvious application of the structures presented in this work. In the last years the interest has been focused on the development of high technological tools for SC acoustic filters. Sánchez-Pérez et al. [29] suggested for the first time an acoustic barrier based on periodic arrangements of rigid scatterers to block audible noise. It has been also shown that natural SC made of periodic arrangement of trees [30] can be used to the same purpose. Optimization techniques [31,32] and resonant scatterers [33] as well as absorbent scatterers [34] were also introduced in the design of these systems to improve their attenuation properties. Recently other structures have been designed including the control of the absorption phenomena [35] as well as the control on the reflections from the ground [36].

The results shown in this work present new possibilities for technological applications due to the tunability of both the periodicity related effects and the resonances of the system. Thus, the arrays could be used to design tunable acoustic filters in the long wavelength regime, being possible the design of tunable SC noise barriers. However, although the SC noise barriers could be wider and more expensive (depending on the materials) than the conventional barriers, they can be attractive for some applications due to transparency to water and wind, tunability of their acoustical properties and seeming aesthetically and more pleasing than the classical ones.

7. Conclusions

In summary, the resonances of a scatterer with complex geometry have been studied both theoretically and experimentally. The analysis needs both the study of a simplified geometry in order to understand the physical origin of the resonances and the numerical solution of the elastic–acoustic problem for the real geometry. Elastic and cavity resonances can be supported by the U-profile scatterer giving rise to attenuation peaks in the low frequency regime of the periodic structure. Therefore such a structure behaves as an acoustic metamaterial with multiple resonances of different physical origin. The theoretical predictions are in good agreement with the experimental results confirming the conclusions about the nature of each resonance. Therefore the models developed can be used to design scatterers with desired resonant frequencies. This gives a possibility of developing periodic structures with multiple tunable stop bands in the low frequency range.

Acknowledgments

This work was supported by MCI Secretaría de Estado de Investigación (Spanish government) and FEDER funds, under Grants MAT2009-09438 and MTM2009-14483-C02-02. V.R.G. is grateful for the support of "Programa de Contratos Post-Doctorales con Movilidad UPV (CEI-01-11)". A.K. and O.U. are grateful for the support of EPSRC (UK) through research Grant EP/E063136/1.

Appendix A. Phenomenological analysis

The complexity of the U-profile geometry motivates the following phenomenological analysis to gain some insight into the nature of the resonances of the U-profiles. We approximate the U-profiles by simple geometries. Thus, we consider an U-profile made of the elastic beams B_1 and B_2 as shown in Fig. A1. The nature of both low attenuation peaks can be understood by analyzing the acoustical properties of basic geometrical shapes such as the rectangular elastic beam B_1 and rectangular cavity generated by the elastic beams B_1 and B_2. In following, the resonances of both the elastic beam (elastic resonances) and the rectangular cavity (cavity resonance) are analyzed.

A.1. Resonances of the elastic beam

Consider a 2D elastic beam (EB) made of LDPF with length l_x and width t_1 (see the schematic view in Fig. A1a) and density ρ. Considering that the EB is fixed at one end (thick solid line in Fig. A1a), the vibration modes can be analyzed by

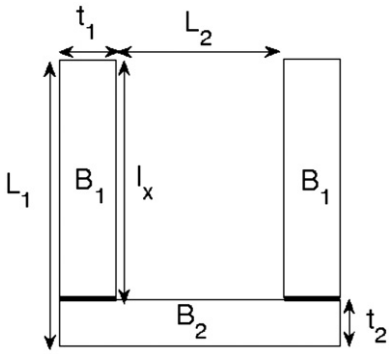

Fig. A1. A simplified geometry of the U-profile used in the phenomenological analysis. B_1 and B_2 are rectangular elastic beams.

Table A1
Relative difference between analytical and numerical results $((f_{\mathrm{COMSOL}}-f_{\mathrm{analytic}})/f_{\mathrm{COMSOL}}\times 100)$.

$t_1 l_x^{-1}$	Euler Bernoulli, f (Hz)	COMSOL, f (Hz)	Relative error (%)
0.01	45.7	45.8	0.22
0.05	229	228.4	0.26
0.1	458	455	0.65
0.15	687	677	1.47
0.2	916	892.9	2.58
0.3	1373	1300.5	5.57
0.5	2289	1998.7	14.52
0.75	3434	2653.6	29.41

means of the following equation as in Refs. [37–39]:

$$EI\frac{\partial^4 v(x)}{\partial x^4} = -\lambda_m \omega_n^2 v(x), \tag{A.1}$$

where $\lambda_m = \rho l_x t_1$ is the linear mass density of the EB, E is Young's modulus, ω_n is the angular frequency of the mode n related to the frequency as $\omega_n = 2\pi f_n$ and I is the second moment of inertia. Harmonic time dependence in the form $e^{-\imath\omega t}$ is assumed. The EI product is known as flexural rigidity.

The eigenfrequencies of the EB can be obtained from the following equation:

$$\cos(k_n l_x)\cosh(k_n l_x)+1=0, \tag{A.2}$$

where $k_n = \sqrt[4]{\omega_n^2 \rho l_x t_1/EI}$.

For the beam made of LDPF, the resonance frequencies of the first and second modes are $f_1=693.8$ Hz ($k_1=28.41$ m^{-1}) and $f_2=4348$ Hz ($k_2=71.12$ m^{-1}), respectively. Using Taylor's series, it is possible to approximate the first mode as

$$k_1 \simeq \frac{\sqrt[4]{12}}{l_x}. \tag{A.3}$$

This first low frequency is particularly interesting for this work.

For further confirmation of this analytical approximation, we have compared the results obtained for the first resonance peak with those obtained using COMSOL for several values of width–length ratio ($t_1 l_x^{-1}$). These values and the relative differences between them are shown in Table A1. For the width–length ratio less than 0.15 the Euler–Bernoulli equation gives the resonant frequency of the EB within 1 percent of the COMSOL results.

A.2. Cavity resonances

Another interesting property of U-profiles is the cavity resonance. The effect of cavity resonators in periodic structures has been analyzed in several publications, showing low frequency stop bands produced by Helmholtz or split-ring resonators as well as the BG corresponding to the periodicity [40,41].

The cavity of the U-profile has dimensions equal to $l_x=0.066$ m and $L_2=0.04$ m as shown in Fig. A1. It can be assumed for simplicity that the walls of the U-profile are perfectly rigid. Thus, Neumann boundary conditions should be applied at the boundaries, and Dirichlet conditions at the open side of the U-profile. The solution of the eigenvalue problem gives a fundamental mode with frequency $f_r = c_{\mathrm{air}}/(4l_x)$. However, due to the fact that the air immediately outside the end of the cavity takes part in the acoustic oscillations, the cavity appears to be somewhat longer than its physical size. This gives rise

to a shift of the resonance. The end correction of the cavity [42] is used to account for this effect. In order to compute the correct resonant frequency, this effective cavity length and the corresponding frequency correction have to be considered. A more rigorous analysis of the cavity would be required to find the exact resonant frequencies, but it has been assumed that the resonance is affected by the end correction of the U-profile cavity as follows:

$$f_r = \frac{c_{\text{air}}}{4(l_x+\delta)}, \tag{A.4}$$

where δ is the end correction. The end correction obtained by Norris et al. in Ref. [42] for cylindrical rigid resonators is

$$\delta \simeq \frac{2a\alpha}{\pi}\log\left(\frac{2}{\alpha}\right), \tag{A.5}$$

where α is the angle of the aperture of the cylindrical Helmholtz resonator and a the radius of the cavity. Taking into account that the resonant frequency of the 2D Helmholtz resonators depends on both the area and the aperture of the cavity, this formula has been adapted to the case of a cylindrical resonator with the same area and aperture as the U-profile. Then the equivalent radius and aperture angle are

$$a_e = \sqrt{\frac{l_x L_2}{\pi}}, \tag{A.6}$$

$$\alpha_e = 2\arcsin\left(\frac{L_2}{2a_e}\right). \tag{A.7}$$

These definitions need additional conditions that make the aperture angle α_e real. The condition $|\sin(\alpha_e/2)| \le 1$ that gives $L_2 \le 4l_x/\pi$. With this, the end correction follows:

$$\delta \simeq \frac{2a_e\alpha_e}{\pi}\log\left(\frac{2}{\alpha_e}\right). \tag{A.8}$$

Using this approximation, the cavity of dimensions previously shown support the first resonance at $f_r = 1155$ Hz.

References

[1] V. Veselago, The electrodynamics of substances with simultaneously negative values of ϵ and μ, *Uspekhi Fizicheskikh Nauk* 92 (1967) 517.
[2] D.R. Smith, W.J. Padilla, D.C. Vier, S.C. Nemat-Nasser, S. Schultz, Composite medium with simultaneously negative permeability and permittivity, *Physical Review Letters* 84 (18) (2000) 4184.
[3] R.A. Shelby, D.R. Smith, S. Schultz, Experimental verification of a negative index of refraction, *Science* 292 (2001) 77.
[4] Z. Liu, X. Zhang, Y. Mao, Y. Zhu, Z. Yang, C. Chan, P. Sheng, Locally resonant sonic materials, *Science* 289 (2000) 1734.
[5] N. Fang, D. Xi, J. Xu, M. Ambati, W. Srituravanich, C. Sun, X. Zhang, Ultrasonic metamaterials with negative modulus, *Nature Materials* 5 (2006) 452.
[6] D. Torrent, A. Hakansson, F. Cervera, J. Sánchez-Dehesa, Homogenization of two-dimensional cluster of rigid rods in air, *Physical Review Letters* 96 (2006) 204302.
[7] D. Torrent, J. Sánchez-Dehesa, Acoustic metamaterials for new two-dimensional sonic devices, *New Journal of Physics* 9 (2007) 323.
[8] S. Guenneau, A. Movchan, G. Pétursson, S.A. Ramakrishna, Acoustic metamaterial for sound focusing and confinement, *New Journal of Physics* 9 (2007) 399.
[9] R. Martínez-Sala, J. Sancho, J.V. Sánchez, V. Gómez, J. Llinares, F. Meseguer, Sound attenuation by sculpture, *Nature* 378 (1995) 241.
[10] M. Sigalas, E. Economou, Elastic and acoustic wave band structure, *Journal of Sound and Vibration* 158 (1992) 377.
[11] M. Kushwaha, P. Halevi, L. Dobrzynski, B. Djafari-Rouhani, Acoustic band structure of periodic elastic composites, *Physical Review Letters* 71 (13) (1993) 2022.
[12] J.V. Sánchez-Pérez, D. Caballero, R. Martínez-Sala, C. Rubio, J. Sánchez-Dehesa, F. Meseguer, J. Llinares, F. Gálvez, Sound attenuation by a two-dimensional array of rigid cylinders, *Physical Review Letters* 80 (24) (1998) 5325.
[13] Ping Sheng, Jun Mei, Zhengyou Liu, Weijia Wen, Dynamic mass density and acoustic metamaterials, *Physica B* 394 (2007) 256–261.
[14] R. Sainidou, B. Djafari-Rouhani, Y. Pennec, J.O. Vasseur, Locally resonant phononic crystals made of hollow spheres or cylinders, *Physical Review B* 73 (2006) 024302.
[15] H. Larabi, Y. Pennec, B. Djafari-Rouhani, J.O. Vasseur, Multicoaxial cylindrical inclusions in locally resonant phononic crystals, *Physical Review E* 75 (2007) 066601.
[16] M. Turkmen, S. Aksu, A.E. etin, A. Ali Yanik, H. Altug, Multi-resonant metamaterials based on UT-shaped nano-aperture antennas, *Optics Express* 19 (8) (2011) 7921.
[17] Y. Lai, Y. Wu, P. Sheng, Z.Q. Zhang, Hybrid elastic solids, *Nature Materials* 10 (2011) 620–624.
[18] J. Berenguer, A perfectly matched layer for the absorption of electromagnetic waves, *Journal of Computer Physics* 114 (1994) 185.
[19] Rayisa P. Moiseyenko, Vincent Laude, Material loss influence on the complex band structure and group velocity in phononic crystals, *Physical Review B* 83 (2011) 064301.
[20] Mahmoud I. Hussein, Theory of damped Bloch waves in elastic media, *Physical Review B* 80 (2009) 212301.
[21] V. Leroy, A. Bretagne, M. Fink, H. Williaime, P. Tabeling, A. Tourin, Design and characterization of bubble phononic crystals, *Applied Physics Letters* 95 (2009) 171904.
[22] Edwin L. Thomas, Applied physics: *bubbly but quiet*, *Nature* 462 (2009) 990.
[23] J.Y. Chung, D.A. Blaster, Transfer function method of measuring in-duct acoustic properties. I. Theory, *Journal of the Acoustical Society of America* 68 (3) (1980) 907–913;
J.Y. Chung, D.A. Blaster, Transfer function method of measuring in-duct acoustic properties. II. Experiment, *Journal of the Acoustical Society of America* 68 (3) (1980) 914–921.
[24] M.K. Nielsen, R.D. Krieg, H.L. Schreyer, A constructive theory for rigid polyurethane foam, *Polymer Engineering and Science* 35 (5) (1995) 387–394.
[25] Yong Mun Seo, Jong Jin Park, Seung Hwan Lee, Choon Mahn Park, Chul Koo Kim, Sam Hyeon Lee, Acoustic metamaterial exhibiting four different sign combinations of density and modulus, *Journal of Applied Physics* 111 (2012) 023504.
[26] J. Li, C. Chan, Double-negative acoustic metamaterial, *Physical Review E* 70 (2004) 055602.

[27] X. Hu, K. Ho, C. Chan, J. Zi, Homogenization of acoustic metamaterials of Helmholtz resonators in fluid, *Physical Review B* 77 (2008) 172301.
[28] L.M. Behovskikh, *Waves in Layered Media*, Academic, New York, 1980.
[29] J.V. Sánchez-Pérez, C. Rubio, R. Martínez-Sala, R. Sánchez-Grandia, V. Gómez, Acoustic barriers based on periodic arrays of scatterers, *Applied Physics Letters* 81 (2002) 5240.
[30] R. Martínez-Sala, C. Rubio, L.M. Garcia-Raffi, J.V. Sánchez-Pérez, E. Sánchez-Pérez, J. Llinares, Control of noise by trees arranged like sonic crystals, *Journal of Sound and Vibration* 291 (2006) 100.
[31] V. Romero-García, E. Fuster, L.M. Garcia-Raffi, E.A. Sánchez-Pérez, M. Sopena, J. Llinares, J.V. Sánchez-Pérez, Band gap creation using quasiordered structures based on sonic crystals, *Applied Physics Letters* 88 (2006) 174104.
[32] E. Fuster-Garcia, V. Romero-García, L.M. Garcia-Raffi, J.V. Sánchez-Pérez, Targeted BG creation using mixed sonic crystal arrays including resonators and rigid scatterers, *Applied Physics Letters* 90 (2007) 244104.
[33] A. Krynkin, O. Umnova, A. Chong, S. Taherzadeh, K. Attenborough, Predictions and measurements of sound transmission through a periodic array of elastic shells in air, *Journal of the Acoustical Society of America* 128 (6) (2010) 3496–3506.
[34] O. Umnova, K. Attenborough, C.M. Linton, Effects of porous covering on sound attenuation by periodic arrays of cylinders, *Journal of the Acoustical Society of America* 119 (2006) 278–284.
[35] V. Romero-García, J.V. Sánchez-Pérez, L.M. Garcia-Raffi, Tunable wideband bandstop acoustic filter based on two-dimensional multiphysical phenomena periodic systems, *Journal of Applied Physics* 110 (2011) 014904.
[36] V. Romero-García, J.V. Sánchez-Pérez, L.M. Garcia-Raffi, Analytical model to predict the effect of a finite impedance surface on the propagation properties of 2D Sonic Crystals, *Journal of Physics D: Applied Physics* 44 (2011) 265501.
[37] E. Voltera, E. Zachmanoglou, *Dynamics of Vibrations*, Columbus, Charles E. Merril Books, Inc., 1965.
[38] P. Morse, K. Inghard, *Theoretical Acoustics*, MacGraw-Hill, New York, 1968.
[39] J. Gere, S. Timoshenko, *Mechanics of Materials*, 4th ed. PWS Publishing Company, Boston, 1997.
[40] A.B. Movchan, S. Guenneau, Split-ring resonators and localized modes, *Physical Review B* 70 (2004) 125116.
[41] X. Hu, C.T. Chan, Jian Zi, Two-dimensional sonic crystals with Helmholtz resonators, *Physical Review E* 71 (2005) 055601. (R).
[42] A.N. Norris, G. Wickham, Elastic Helmholtz resonators, *Journal of the Acoustical Society of America* 93 (2) (1993) 617.